

https://doi.org/10.1070/QEL17259

Rabi spectroscopy of the clock transition in thulium atoms in a one-dimensional optical lattice

E.S. Fedorova, D.O. Tregubov, A.A. Golovizin, D.A. Mishin,
D.I. Provorchenko, K.Yu. Khabarova, V.N. Sorokin, N.N. Kolachevsky

Abstract. **The clock transition at a wavelength of 1.14 μm in thulium atoms in an optical lattice in the Lamb–Dick regime is studied. The capture of thulium atoms makes it possible to suppress completely both the transition broadening due to the first-order Doppler effect and the shift of the transition frequency caused by the recoil effect. The excitation spectra of sideband oscillation frequencies and Rabi oscillations of population between the clock transition levels upon resonance excitation are investigated.**

Keywords: *optical lattice, sideband frequencies, Lamb–Dicke regime, Rabi oscillations, optical clock, clock transition, ultracold atoms, thulium.*

1. Introduction

Currently, the frequency is one of the most precisely measured physical quantities; the relative precision and stability of frequency references are continuously improved. The relative precision at 1 part in 10^{18} [1, 2] opens up a wide range of possibilities of using frequency standards in the optical range to solve a number of fundamental [3, 4] and applied [5] problems. Since transportable frequency standards are often called for, along with stationary optical clocks, compact systems (insensitive to external perturbations) are being developed throughout the world [6–9]. A promising element for designing a transportable optical clock is thulium, which demonstrates extremely low (for neutral atoms) sensitivity to thermal radiation of the environment and external static electrical fields [10].

In most of optical clocks based on neutral atoms the latter are captured into an optical lattice [11], within which atoms are localised in space along a certain direction at distances smaller than the excitation wavelength; this arrangement makes it possible to suppress completely the recoil effect and the first-order Doppler effect (Lamb–Dicke regime [12]). The reason is as follows: the velocity of an atom in a confining potential ceases to be a continuous variable, and its motion is described by an oscillatory state. As a result, when studying a transition of an atom in a confining potential, one observes not a Doppler-broadened line but a discrete absorption spectrum, consisting of lines spaced by the vibrational frequency ν_z (it is assumed that the natural transition width γ is small in comparison with the oscillation frequency ν_z and that the transitions with a change in the vibrational quantum number are spectrally resolvable). The probability of the transitions with a change in the vibrational quantum number is determined by the Lamb–Dicke parameter $\eta = 2\pi z_0/\lambda_c$, i.e., by the ratio of the characteristic size of the wave function in the ground vibrational state z_0 to the excitation wavelength λ_c [12]. In the limit $\eta \ll 1$ (Lamb–Dicke regime) the transitions at sideband frequencies are significantly suppressed.

The study of the spectrum of a clock transition in an optical lattice is an important stage in developing optical clocks; in particular, it is a way of measuring the distribution of atoms over vibrational sublevels and determining decoherence sources. In this study we consider the Rabi spectroscopy of the clock transition $|4f^{13}(^2F^o)6s^2, J = 7/2\rangle \rightarrow |4f^{13}(^2F^o)6s^2, J = 5/2\rangle$ at the wavelength $\lambda_c = 1.14$ μm in thulium atoms in an optical lattice, in the Lamb–Dicke regime at spectrally resolvable sideband frequencies.

2. Experimental setup

To form a cloud of ultracold thulium atoms, we used a magneto-optical trap (MOT) with two cooling stages [13], which provides capture of up to 10^6 atoms at a temperature of 15 μK (Fig. 1). After the end of cooling cycle atoms are recaptured into a one-dimensional optical lattice at a magic wavelength of 813.32 nm [14], and the central magnetic component of the clock transition $|J = 7/2, F = 4, m_F = 0\rangle \rightarrow |J = 5/2, F = 3, m_F = 0\rangle$ is excited in it. The radiation source for exciting the clock transition is a semiconductor laser, frequency-stabilised to an external high-Q cavity [made of ULE (ultra low expansion) glass] by the Pound–Drever–Hall method [15]. The clock laser radiation was fed into a vacuum chamber through a polarisation-maintaining optical fibre and aligned with the beam forming the optical lattice on a polarisation beam splitter. The focal length and position of the objective at the fibre output were chosen such as to make the clock laser beam at the centre of vacuum chamber be collimated and have a size greatly exceeding the atomic cloud size.

To remove the magnetic sublevel degeneracy, a uniform magnetic field $B_0 = 0.45$ G was switched on for the excitation time of clock transition; this field, directed horizontally and perpendicular to the optical lattice axis, specified the quantisation axis in the system under consideration. The optical lat-

E.S. Fedorova, K.Yu. Khabarova, V.N. Sorokin, N.N. Kolachevsky
Lebedev Physical Institute, Russian Academy of Sciences, Leninsky prosp. 53, 119991 Moscow, Russia; Russian Quantum Center, Bol'shoi bul'var 30, stroenie 1, Skolkovo, 121205 Moscow, Russia; e-mail: fedorova.e.s@outlook.com;
D.O. Tregubov, A.A. Golovizin, D.A. Mishin, D.I. Provorchenko
Lebedev Physical Institute, Russian Academy of Sciences, Leninsky prosp. 53, 119991 Moscow, Russia

Received 11 February 2020
Kvantovaya Elektronika **50** (3) 220–224 (2020)
Translated by Yu.P. Sin'kov

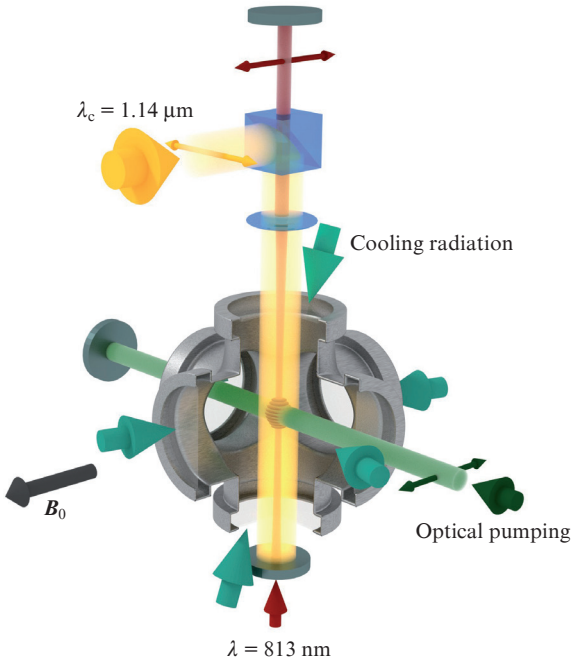

Figure 1. (Colour online) Schematic of the experimental setup: (red) optical lattice radiation, (yellow) excitation radiation of clock transition, (green) optical pumping radiation, and (turquoise) cooling radiation. The gray arrow shows the direction of magnetic field $\boldsymbol{B}_0$. Thin arrows indicate the beam polarisation.

tice radiation is linearly polarised, and its electrical component is parallel to the magnetic field $\boldsymbol{B}_0$. The clock laser radiation is also linearly polarised, and its magnetic component is oriented along the magnetic field. Since the clock transition under study is a magnetic dipole transition, this configuration allows one to excite π transitions. To amplify the excitation signal of the clock transition, atoms were prepared in the state with $m_F = 0$ using optical pumping, which was discussed in detail in [16].

3. Clock transition spectroscopy

3.1. Sideband frequencies

Absorption spectra were measured by scanning the clock radiation frequency near the resonance value (corresponding to the clock transition) using an acousto-optic modulator; the excitation probability was found from the fraction of atoms remaining in the ground state. The clock transition was excited by a short pulse (τ = 2 ms), whose intensity greatly exceeded the intensity necessary for forming a π pulse of duration τ. The high excitation radiation intensity made it possible to increase the excitation probability of transitions with a change in the vibrational quantum number; in this case, the central line corresponding to the transitions without a change in this parameter was saturated under these conditions.

One of the obtained clock transition spectra in the Lamb–Dicke regime with spectrally resolvable sideband frequencies is shown in Fig. 2a. It can be seen that the sideband resonances, corresponding to the excitation of clock transition with a simultaneous change in the vibrational quantum number by unity, have a pronounced asymmetric shape. This shape of sideband resonances, typical of experiments with cold atoms in optical lattices [17, 18], is related to the lattice potential anharmonicity.

A model describing the shape of sideband resonance lines for a one-dimensional optical lattice was presented in [19]. The total excitation probability of an electronic transition with a change in the longitudinal vibrational quantum number by +1 (–1) in dependence of the excitation radiation detuning δ (on the assumption of thermal distribution of atoms over vibrational states) is described by the expression

$$p_{+1(-1)}(\delta) \propto \sum_{n_z=0(1)}^{N_z} \exp\left(-\frac{E_{n_z}}{k_B T_z}\right) p^{(n_z)}(\delta), \quad (1)$$

where n_z is the number of the vibrational state corresponding to the longitudinal motion of atoms in the lattice, N_z is the total number of longitudinal vibrational states in the potential trap, k_B is the Boltzmann constant, T_z is the temperature of the distribution of atoms over longitudinal vibrational states, and; E_{n_z} is the atomic energy corresponding to the longitudinal vibrational state n_z (disregarding the coupling with transverse modes). The probability of exciting an electronic transition with a change in the longitudinal vibrational quantum number by ±1 for the state n_z can be written as [19]

$$p^{(n_z)}(\delta) \propto \frac{\kappa^2}{\zeta(n_z)}\left[1 - \frac{\delta}{\zeta(n_z)}\right]$$

$$\times \exp\left\{-\kappa\left[1 - \frac{\delta}{\zeta(n_z)}\right]\right\} \Theta[\zeta(n_z) - \delta], \quad (2)$$

where

$$\kappa = \frac{\zeta(n_z)}{\nu_{rec}} \frac{h\nu_z}{k_B T_r}; \quad \zeta(n_z) = \nu_z - \nu_{rec}(n_z + 1),$$

$\Theta(x)$ is the Heaviside function, T_r is the temperature of the distribution of atoms over the vibrational states corresponding to the transverse atomic motion in the lattice, $\nu_{rec} = h \times (2\lambda^2 m)^{-1}$ is the recoil frequency, λ is the wavelength of the radiation forming the optical lattice, m is the atomic mass, and h is Planck's constant. The recoil frequency for thulium atoms in an optical lattice at a wavelength of λ = 813.3 nm is ν_{rec} = 1.8 kHz.

We approximated the shape of the experimentally obtained lines by expression (1); determined the atomic temperature, assuming it to be the same for longitudinal and transverse vibrational states; and measured the longitudinal vibrational frequencies of the optical lattice, ν_z (Fig. 2a). For example, for an optical lattice of depth $U = 344E_{rec}$ ($E_{rec} = h\nu_{rec}$ is the recoil energy), we found that the atomic temperature is $T = 11 \pm 2$ μK and the longitudinal vibration frequency is $\nu_z = 60 \pm 2$ kHz. The longitudinal vibration frequency can be expressed in terms of the trap parameters as

$$\nu_z = \frac{4}{w_0 \lambda}\sqrt{\frac{2a_0^3 \alpha P_c}{cm}}, \quad (3)$$

where w_0 is the waist radius (w_0 = 126 μm in our experiment), P_c is the power of radiation forming the optical lattice, a_0 is the Bohr radius, and c is the speed of light; the polarisability α is taken in atomic units. Thus, based on the dependence of lattice vibrational frequencies ν_z on power (see Fig. 2b), one

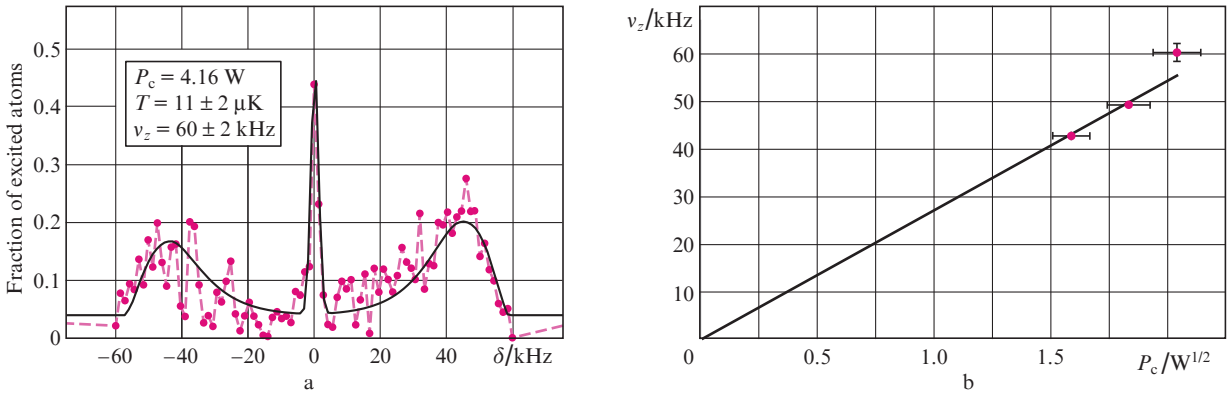

Figure 2. (a) Spectrum of the clock transition in the Lamb–Dicke regime at spectrally resolvable sideband frequencies and optical lattice depth $U = 344E_{rec}$ (the solid line is an approximation of the sideband frequencies by expression (1) for the high- and low-frequency wings and by a Lorenzian for the central resonance) and (b) dependence of the oscillation frequencies of thulium atoms in a confining potential in the direction of the optical lattice axis on the power P_c of the radiation forming the optical lattice (the solid line is an approximation of experimental data by the function $y = \beta x$).

can determine the dynamic polarisability of the central magnetic sublevel of the ground state: $\alpha = 139 \pm 7$ au. The calculations showed that the contribution of the tensor polarisability α_t for the central magnetic sublevel of thulium atom at $\lambda = 813.32$ nm is 3 au; in sum, the scalar polarisability $\alpha_s = 136 \pm 7$ au, which is in agreement with the value obtained previously from the spectrum of parametric resonances: $\alpha_s = 146 \pm 44$ au [14].

The fairly high atomic temperature in the optical lattice may lead to spectral broadening of the clock transition and limit the excitation efficiency due to the dephasing of Rabi oscillations for the atoms in different vibrational states (see below). Indeed, the mean value of vibrational quantum number at an atomic temperature T is given by the expression

$$\bar{n}_z = \left[\exp\left(\frac{h\nu_z}{k_B T}\right) - 1\right]^{-1}. \quad (4)$$

At a temperature $T = 11$ μK the mean value is $\bar{n}_z = 3.3,$, which corresponds (at a total number of vibrational levels $N_z = 10$) to a rather high population of all vibrational states.

3.2. Dephasing of Rabi oscillations

When exciting a transition in an atom by resonance radiation ($\delta = 0$), the upper-level population is described by Rabi oscillations:

$$p_e(n_z, n_r, t) = \sin^2(\pi\Omega_{n_z n_r} t). \quad (5)$$

The Rabi frequency $\Omega_{n_z n_r}$ depends on the atomic vibrational states n_z and n_r. For the transition without a change in the vibrational quantum number, the Rabi frequency has the form [19]

$$\Omega_{n_z n_r} = \Omega_0 \exp\left(-\frac{\eta_z^2}{2}\right)\exp\left(-\frac{\eta_r^2}{2}\right) L_{n_z}(\eta_z^2) L_{n_r}(\eta_r^2). \quad (6)$$

Here η_z and η_r are the Lamb–Dicke parameters for the longitudinal and transverse degrees of freedom, respectively; Ω_0 is the Rabi frequency for a stationary atom; and $L_n(x)$ are Laguerre polynomials.

Since one cannot excite a single specific vibrational state in an experiment, the total excitation probability for atoms in all these states is observed. At the initial instant of transition excitation, the Rabi oscillations for the atoms in all vibrational states have the same phase; however, in the course of time, the difference in the Rabi frequencies $\Omega_{n_z n_r}$ leads to a phase difference for population oscillations and damping of the general observed Rabi oscillations for an atomic ensemble.

To obtain a time dependence of the total excitation probability, one must perform summation over all vibrational states with the corresponding weights q_{n_z} and q_{n_r}:

$$P_e(t) = \sum_{n_z, n_r} q_{n_z}(T_z) q_{n_r}(T_r) p_e(n_z, n_r, t). \quad (7)$$

where

$$q_{n_z}(T_z) = \left[1 - \exp\left(-\frac{h\nu_z}{k_B T_z}\right)\right]\exp\left(-\frac{n_z h\nu_z}{k_B T_z}\right);$$

$$q_{n_r}(T_r) = \left[1 - \exp\left(-\frac{h\nu_r}{k_B T_r}\right)\right]\exp\left(-\frac{n_r h\nu_r}{k_B T_r}\right)$$

The radial oscillation frequencies are generally much lower than the confining potential depth: $\nu_r \ll U/h$; therefore, as was shown in [19], the sum over n_r can be considered as a sum of an infinite series. As a result, the total excitation probability is given by the expression

$$P_e(t) = \sum_{n_z}\left\{\frac{1}{2} + \frac{1}{2}\left[1 - \exp\left(-\frac{h\nu_r}{k_B T_r}\right)\right]\right.$$
$$\times\left[\exp\left(-\frac{h\nu_r}{k_B T_r}\right)\cos[\phi(1-\eta_r^2)] - \cos\phi\right]$$
$$\left.\times\left[1 + \exp\left(-\frac{2h\nu_r}{k_B T_r}\right) - 2\exp\left(-\frac{h\nu_r}{k_B T_r}\right)\cos(\phi\eta_r^2)\right]^{-1}\right\}, \quad (8)$$

$$\phi = 2\pi t\Omega_0 \exp\left(-\frac{\eta_z^2}{2}\right)\exp\left(-\frac{\eta_r^2}{2}\right) L_{n_z}(\eta_z^2).$$

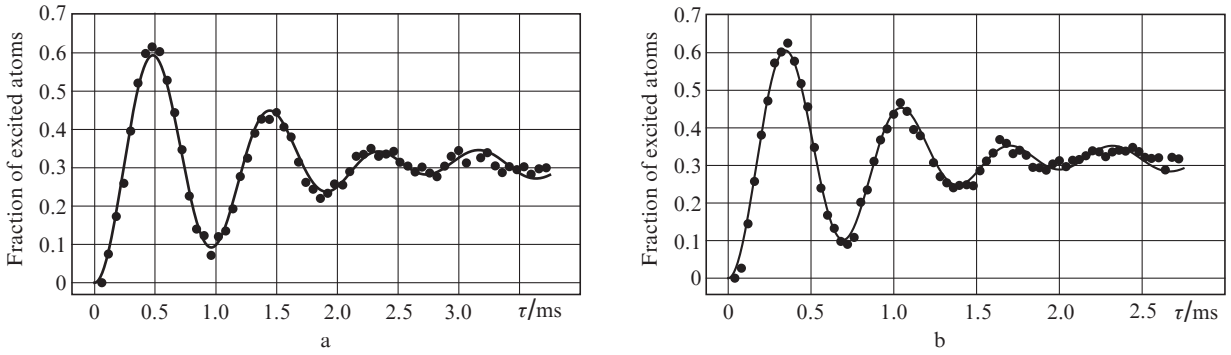

Figure 3. Dependences of the populations of the upper clock level on the excitation pulse duration τ at a wavelength of 1.14 μm for Ω_0 = (a) 1.11 ± 0.01 kHz and (b) 1.51 ± 0.01 kHz. The solid lines are approximations of experimental data by expression (8).

The Rabi oscillations of the upper clock level population upon resonance excitation and their dephasing were observed experimentally. The measurement results and their approximation by expression (8) are given in Fig. 3 for an optical lattice of depth $U = 208E_{\text{rec}}$.

When carrying out an approximation, the parameters ν_z = = 43 kHz and ν_r = = 76 Hz (obtained from the spectra of sideband oscillation frequencies) were fixed, while the Rabi frequency Ω_0; temperature (on the assumption that $T_z = T_r = T$); and longitudinal and transverse Lamb–Dicke parameters, η_z and η_r, were varied. The following optimal parameters were found: T = 11 ± 2 μK, η_z = 0.24 ± 0.01, $\eta_r = (5.5 \pm 0.8) \times 10^{-3}$, and Ω_0 = 1.11± 0.01 kHz and 1.51± 0.01 kHz (for two experiments with different clock-transition excitation intensities). It should be noted that the Lamb–Dicke parameter η_z = 0.24 ± 0.01 found by approximation exceeds the calculated value η_z = 0.14. This discrepancy may be due to the significant anharmonicity of the optical lattice potential in the experiment and necessity of taking into account higher order terms in the expansion of potential in powers. When the excitation beam direction coincides exactly with the optical lattice axis, the Lamb–Dicke parameter for transverse oscillations should be zero (η_r = 0). Its nonzero value is due to the inaccuracy of alignment and relatively high atomic temperature.

Another specific feature of the observed oscillations is that their fast damping (for few milliseconds); this damping time is much shorter than the radiative lifetime of the upper level of clock transition (112 ms). In addition, the decoherence time changes with an increase in excitation intensity, whereas the number of oscillation periods remains constant (Fig. 3). This behaviour is characteristic of the decoherence caused by the dephasing of Rabi oscillations arising upon excitation of different vibrational states. Indeed, time t and Rabi frequency Ω_0 of atom at rest enter expression (8) in the form of a product, and a change in Ω_0 scales the general pattern in time, retaining invariable the relative phases of the terms and, correspondingly, the number of damping periods.

The results reported in Fig. 3 confirm again the relatively high temperature of atoms in the optical lattice and its influence on the clock transition excitation. To reduce this effect, we are planning to use one of deep laser cooling techniques in further experiments, for example, cooling at sideband oscillation frequencies [20], SWAP cooling [21], evaporative cooling by reducing the depth of confining lattice potential [22], or Doppler cooling using a transition with a natural linewidth of ~10 kHz [23].

4. Conclusions

We have present the spectroscopy of the clock transition $|J = 7/2, F = 4, m_F = 0\rangle \rightarrow |J = 5/2, F = 3, m_F = 0\rangle$ in a thulium atom at the wavelength λ_c = 1.14 μm in an optical lattice in the mode of spectrally resolvable sideband frequencies and in the Lamb–Dicke regime. An approximation of the line profile makes it possible to determine the atomic temperature and the optical lattice frequency corresponding to the longitudinal motion of atoms. We also observed Rabi oscillations between clock transition levels under resonance radiation. The high temperature of atoms in the optical lattice leads to dephasing of oscillations and their damping for a time much shorter than the radiative lifetime of the upper clock level. We are planning to reduce the temperature of atoms in the optical lattice in further experiments to observe a more contrast pattern of Rabi oscillations.

Acknowledgements. This work was supported by the Russian Science Foundation (Grant No. 19-12-00137).

References

1. Hinkley N., Sherman J.A., Phillips N.B., Schioppo M., Lemke N.D., Beloy K., Pizzocaro M., Oates C.W., Ludlow A.D. *Science*, **341**, 1215 (2013).
2. Bloom B.J., Nicholson T.L., Williams J.R., Campbell S.L., Bishof M., Zhang X., Zhang W., Bromley S.L., Ye J. *Nature*, **506**, 71 (2014).
3. Chou C.W., Hume D.B., Rosenband T., Wineland D.J. *Science*, **329**, 1630 (2010).
4. Blatt S., Ludlow A.D., Campbell G.K., Thomsen J.W., Zelevinsky T., Boyd M.M., Ye J., Baillard X., Fouché M., Le Targat R., Brusch A., Lemonde P., Takamoto M., Hong F.-L., Katori H., Flambaum V.V. *Phys. Rev. Lett*., **100**, 140801 (2008).
5. Müller J., Dirkx D., Kopeikin S.M., Lion G., Panet I., Petit G., Visser P.N.A.M. *Space Sci. Rev*., **214**, 5 (2018).
6. Arnold K.J., Kaewuam R., Roy A., Tan T.R., Barrett M.D. *Nat. Commun*., **9**, 1650 (2018).
7. Nauta J., Borodin A., Ledwa H.B., Stark J., Schwarz M., Schmöger L., Micke P., López-Urrutia J.R.C., Pfeifer T. *Nucl. Instrum. Methods Phys. Res., Sect. B*, **408**, 285 (2017).
8. Yu Y.-m., Sahoo B.K. *Phys. Rev. A*, **97**, 041403 (2018).
9. Kozlov M.G., Safronova M.S., López-Urrutia J.R.C., Schmidt P.O. *Rev. Mod. Phys*., **90**, 045005 (2018).
10. Golovizin A., Fedorova E., Tregubov D., Sukachev D., Khabarova K., Sorokin V., Kolachevsky N. *Nat. Commun*., **10**, 1724 (2019).

11. Takamoto M., Katori H. *Phys. Rev. Lett*., **91**, 223001 (2003).
12. Bergquist J.C., Itano W.M., Wineland D.J. *Phys. Rev. A*, **36** (1), 428 (1987).
13. Kalganova E., Prudnikov O., Vishnyakova G., Golovizin A., Tregubov D., Sukachev D., Khabarova K., Sorokin V., Kolachevsky N. *Phys. Rev. A*, **96**, 033418 (2017).
14. Kalganova E.S., Golovizin A.A., Shevnin D.O., Tregubov D.O., Khabarova K.Yu., Sorokin V.N., Kolachevsky N.N. *Quantum Electron*., **48** (5), 415 (2018) [*Kvantovaya Elektron*., **48** (5), 415 (2018)].
15. Drever R.W.P., Hall J.L., Kowalski F.V., Hough J., Ford G.M., Munley A.J., Ward H. *Appl. Phys. B*, **31** (2), 97 (1983).
16. Fedorova E.S., Tregubov D.O., Golovizin A.A., Vishnyakova G.A., Mishin D.A., Provorchenko D.I., Khabarova K.Yu., Sorokin V.N., Kolachevsky N.N. *Quantum Electron*., **49** (5), 418 (2019) [*Kvantovaya Elektron*., **49** (5), 418 (2019)].
17. Brusch A., Le Targat R., Baillard X., Fouché M., Lemonde P. *Phys. Rev. Lett*., **96** (10), 103003 (2006).
18. Bober M., Morzyński P., Cygan A., Lisak D., Masłowski P., Prymaczek M., Wcisło P., Ablewski P., Piwiński M., Wójtewicz S. *Meas. Sci.Technol.*, **26** (7), 075201 (2015).
19. Blatt S.,Thomsen J.W., Campbell G.K., Ludlow A.D., Swallows M.D., Martin M.J., Boyd M.M., Ye J. *Phys. Rev. A*, **80** (5), 052703 (2009).
20. Wineland D.J., Itano W.M. *Phys. Rev. A*, **20** (4), 1521 (1979).
21. Petersen N., Mühlbauer F., Bougas L., Sharma A., Budker D., Windpassinger P. *Phys. Rev. A*, **99**, 063414 (2019).
22. Ketterle W., VanDruten N.J. *Adv. At. Mol. Opt. Phys*., **37**, 181 (1996).
23. Berglund A.J., Hanssen J.L., McClelland J.J. *Phys. Rev. Lett*., **100** (11), 113002 (2008).